BAMS Article

Global Patterns of Hottest, Coldest, and Extreme Diurnal Variability on Earth

Yunxia Zhao, Hamid Norouzi, Marzi Azarderakhsh, and Amir AghaKouchak

ABSTRACT: Most previous studies of extreme temperatures have primarily focused on atmospheric temperatures. Using 18 years of the latest version of the Moderate Resolution Imaging Spectroradiometer (MODIS) land surface temperature (LST) data, we globally investigate the spatial patterns of hot and cold extremes as well as diurnal temperature range (DTR). We show that the world's highest LST of 80.8°C, observed in the Lut Desert in Iran and the Sonoran Desert in Mexico, is over 10°C above the previous global record of 70.7°C observed in 2005. The coldest place on Earth is Antarctica with the record low temperature of –110.9°C. The world's maximum DTR of 81.8°C is observed in a desert environment in China. We see strong latitudinal patterns in hot and cold extremes as well as DTR. Biomes worldwide are faced with different levels of temperature extremes and DTR: we observe the highest zonal average maximum LST of 61.1° ± 5.3°C in the deserts and xeric shrublands; the lowest zonal average minimum LST of −66.6° ± 14.8°C in the tundra; and the highest zonal average maximum DTR of 43.5° ± 9.9°C in the montane grasslands and shrublands. This global exploration of extreme LST and DTR across different biomes sheds light on the type of extremes different ecosystems are faced with.

KEYWORDS: Climate change; Climate variability; Surface temperature; Diurnal effects

https://doi.org/10.1175/BAMS-D-20-0325.1
Corresponding author: Yunxia Zhao, yunxiaz1@uci.edu
Supplemental material: https://doi.org/10.1175/BAMS-D-20-0325.2
In final form 27 April 2021

AFFILIATIONS: **Zhao**—Department of Civil and Environmental Engineering, University of California, Irvine, Irvine, California; **Norouzi**—New York City College of Technology, City University of New York, Brooklyn, New York; **Azarderakhsh**—School of Computer Science and Engineering, Fairleigh Dickinson University, Teaneck, New Jersey; **AghaKouchak**—Department of Civil and Environmental Engineering, and Department of Earth System Science, University of California, Irvine, Irvine, California

While the Earth has warmed by around 1°C on average above the preindustrial level, much higher record hot extremes have been observed around the world in the past decades (IPCC 2018). Ecoregions worldwide are showing signs of thermal stress, leading to changes in their structure, composition, functioning, and significant ecological pressure (Hughes et al. 2018; Peng et al. 2013; Xie et al. 2018). Between 1980 and 2018, over 2,000 extreme events including heatwaves, droughts, wildfires, and winter storms have occurred, killing over 180,000 people and leading to nearly $700 billion in damage (Munich RE 2019). Most previous studies on temperature variability have focused on extreme air temperatures (e.g., heatwaves) (Schwartz 2005; Oudin Åström et al. 2013; Kretschmer et al. 2018; Papritz 2020; Luo et al. 2019; Johnson et al. 2018; Kodra et al. 2011; Tang et al. 2013) and relatively little attention has been paid to extreme high and low temperatures across the Earth's skin (Azarderakhsh, et al. 2020; Nie et al. 2020).

Studies of extreme hot land surface temperatures (LSTs), also known as skin temperature, have mainly focused on the city or subcity scale where the urban heat island is a major hazard (Benz et al. 2021). However, the most extreme hot and cold LSTs usually occur in deserts and polar regions, respectively. Warming rates in arid areas are higher than the global average (Zhou et al. 2015; Zhou and Wang 2016), and the Arctic region is warming at a rate more than twice the global mean (Cohen et al. 2014).

Locations of the hottest and coldest places on Earth's have always been of interest to a broad range of scientists including meteorologists, ecologists, and biologists. A global understanding of extreme hot and cold LSTs and diurnal temperature ranges (DTRs, daily maximum LST minus daily minimum LST) across different environments and biomes could shed light on the type of extremes different ecosystems are faced with. This is increasingly more important as the atmosphere warms in response to anthropogenic emissions. However, there are limited temperature observations in the polar regions and desert environments where the most extreme temperatures occur.

According to the World Meteorological Organization (WMO) Commission of Climatology (CCl) World Archive of Weather and Climate Extremes, the record high atmospheric temperature is 56.7°C observed in Death Valley on 10 July 1913, and the record low temperature is −89.2°C observed in Antarctica on 21 July 1983 (Arizona State University 2020). However, the limited coverage of ground-based observations indicates that the hottest and coldest spots reported by WMO are likely not the actual hottest and coldest places on Earth. Further, the land surface temperature is expected to be warmer than atmospheric temperature (Mildrexler et al. 2011a; Good 2016). The Moderate Resolution Imaging Spectroradiometer (MODIS) provides LST data with global coverage at high resolution collected twice daily, which can be used to identify the global hot and cold spots. The quality of V5 MODIS LST data has been widely validated in literature (Coll et al. 2005, 2009; Wan 2008; Wan et al. 2004; Wan and Li 2008; Wang and Liang 2009; Li et al. 2013; Wang et al. 2007), with an accuracy of within ±2 K (±1 K in most cases) for all the validation sites except bare soil sites. Mildrexler et al. (2011b) investigated LST from 2003 to 2009 using an early version of MODIS LST data. To avoid the effects of wildfires in vegetated areas, Mildrexler et al. focused on barren areas and open shrublands instead of a global analysis. They identified the Lut Desert (also known as the Dasht-e Lut) in Iran to be the world's hottest place with a record high temperature of 70.7°C observed in

2005. However, Wan (2014) raised concerns about the underestimation of the LST by the V5 MODIS LST (version 5) data over bare soil, where LSTs are underestimated by more than 2 K and up to 4.5 K. For this reason, we hypothesized that the record high temperature detected by Mildrexler et al. in the Lut Desert is likely underestimated.

In a recent development, NASA released the *Aqua* MODIS LST MYD11A1 version 6 product with an improved algorithm for detecting land surface temperatures (Wan et al. 2015) at 1-km resolution. The improved resolution [1 km versus 5.6 km used in Mildrexler et al. (2011b)] and algorithm confirmed more accurate land surface temperatures including over bare soils. Compared with V5 MODIS LST, the accuracy of V6 MODIS LST has been improved from up to ±4.5 K to within ±1 K at most of the validation sites (Wan 2014; Duan et al. 2019). The newest V6 MODIS LST product has been freely available since 2016 (Duan et al. 2018). With the latest high-resolution (1 km) V6 MODIS LST data available, we have investigated not only record high, but also record low and maximum diurnal temperature range around the world. Here we searched for daily and yearly maximum (daytime) and minimum (nighttime) LSTs and maximum DTRs across the globe from 2002 to 2019. We also investigated the overall maximum and minimum LSTs and maximum DTRs during the entire record. Further, we estimated zonal averages and extreme values of the 18-yr maximum and minimum LSTs and maximum DTRs for different biomes based on the global map of biomes (Dinerstein et al. 2017) (Fig. ES1).

Materials and methods

Land surface temperature data. MODIS on board the *Aqua* satellite provides LST (from MYD11A1 V6) (Wan et al. 2015) estimates with 1-km spatial resolution for clear-sky conditions at 1330 and 0130 local solar time, which are close to the times when daily maximum and minimum temperatures occur. We note, however, that the actual daily minimum (maximum) temperature may occur sometime before or after 0130 (1330) local solar time (Sharifnezhadazizi et al. 2019). We extracted LST data from 4 July 2002 to 31 December 2019. According to the quality control (QC) information (Wan 2013), only high-quality data with average LST error ≤ 1 K were included in our analysis.

It should be noted that the yearly maximum and minimum LSTs and yearly maximum DTR observed in 2002 may be underestimated since observations begin on 4 July 2002, yet higher temperature extremes may have occurred before July. Additionally, we have only used one decimal degree of the temperature observations as considering two digits of accuracy for satellite-based temperature data are not warranted.

Fire data. Due to residual effects of fire disturbance over the post-fire period (Liu et al. 2019), the LST of post-fire areas tends to be higher than the normal temperature and consequently leads to the erroneous recording of the daily maximum LST. Therefore, to avoid the effects of wildfires, we used the *Aqua* MODIS MYD14A1 Thermal Anomalies and Fire Daily 1-km Global V006 data product (Giglio et al. 2016) to exclude pixels that have been flagged as fire at any of the three fire classes (low-confidence fire, nominal-confidence fire, or high-confidence fire) from 2002 to 2019. In addition, we excluded 9 out of 6389 global daily maximum LST observations from analysis, because they were detected in the high latitudes and the Amazon forest, where most of the global daily maximum LST observations do not occur. These nine observations are very close to the burned areas as determined by MODIS MYD14A1. It is possible that these observations may have been affected by nearby fires. Therefore, we removed them from our study.

Biome data. We used the RESOLVE Ecoregions dataset (Dinerstein et al. 2017) to extract LST individually from each of the 14 biomes including tropical and subtropical moist broadleaf forests; tropical and subtropical dry broadleaf forests; tropical and subtropical coniferous forests; temperate broadleaf and mixed forests; temperate conifer forests; boreal forests/taiga; tropical

and subtropical grasslands, savannas, and shrublands; temperate grasslands, savannas, and shrublands; flooded grasslands and savannas; montane grasslands and shrublands; tundra; Mediterranean forests, woodlands, and scrub; deserts and xeric shrublands; and mangroves.

Global analysis of temperature extremes and diurnal temperature range. To identify the hottest, coldest, and most diurnally variable spots, we searched for daily and yearly maximum and minimum LSTs and maximum DTRs across the globe from 4 July 2002 to 31 December 2019. Further, we estimated 18-yr maximum and minimum LSTs and maximum DTR during the entire research period at each pixel. To investigate latitudinal patterns in these three temperature variables, we individually averaged them by latitude. Besides, to explore the extent to which different biomes are faced with temperature extremes, we estimated zonal averages for each of the 14 biomes.

Results

Results reveal that the Lut Desert in Iran and the Sonoran Desert in Mexico are the hottest places on Earth with an LST of 80.8°C (Fig. 1), which is over 10°C hotter than the world's highest LST of 70.7°C reported in Mildrexler et al. (2011b) and consistent with Azarderakhsh et al. (2020).

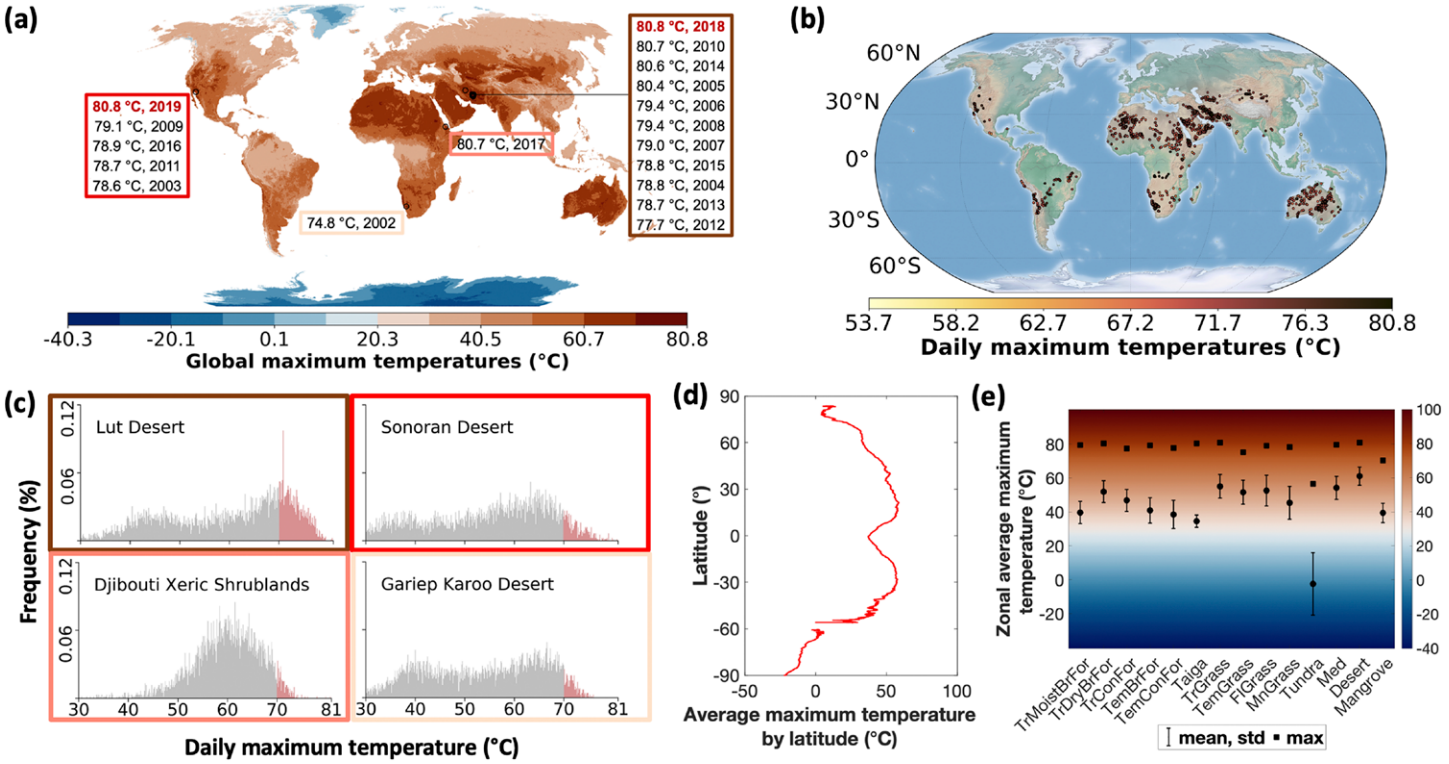

Fig. 1. Global hotspots of the Earth. Locations of the (a) annual and (b) daily maximum LSTs from 4 Jul 2002 to 31 Dec 2019 and (c) histograms showing the frequency distributions of daily maximum LSTs of the four hottest places on Earth during the study period. The red areas indicate temperatures above 70°C. The percentages of days with daily maximum LSTs above 70°C are 25.1%, 8.2%, 4.4%, and 5.2% in the Lut Desert, the Sonoran Desert, the Djibouti xeric shrublands, and the Gariep Karoo Desert, respectively. (d) The average maximum LSTs by latitude, and (e) zonal maximum and average LSTs for each of the 14 biomes: tropical and subtropical moist broadleaf forests (TrMoistBrFor), tropical and subtropical dry broadleaf forests (TrDryBrFor), tropical and subtropical coniferous forests (TrConFor), temperate broadleaf and mixed forests (TemBrFor), temperate conifer forests (TemConFor), boreal forests/taiga (Taiga), tropical and subtropical grasslands, savannas and shrublands (TrGrass), temperate grasslands, savannas and shrublands temperate grasslands, savannas and shrublands (TemGrass), flooded grasslands and savannas (FlGrass), montane grasslands and shrublands (MnGrass), tundra (Tundra), Mediterranean forests, woodlands and scrub (Med), deserts and xeric shrublands (Desert), and mangroves (Mangrove). Error bars indicate standard deviation. Scientific color maps are used in this study to avoid data distortion and visual error (Crameri et al. 2020; Crameri 2018).

The record low LST of –110.9°C observed in Antarctica is approximately 20°C lower than what was reported by WMO as the lowest temperature of –89.2°C (Fig. 2). The world's maximum DTR of 81.8°C is observed in the Qaidam Basin (a desert environment in China) that exhibits an incredible level of variability within a day (Fig. 3). Our analysis also reveals strong latitudinal patterns in the 18-yr maximum and minimum LSTs and maximum DTR, which are attributed to the climate and biophysical regulation. In the following, we discuss our findings in more detail.

Global pattern of daily maximum temperature. We observe the daily maximum LSTs over the globe mainly in two biomes: deserts and xeric shrublands biome and the tropical and subtropical grasslands, savannas, and shrublands biome (see Fig. 1b and the corresponding biomes in Fig. ES1). These two biomes are where the two largest magnitudes of zonal average maximum LSTs of 61.1° ± 5.3°C and 55.0° ± 7.0°C occur (Fig. 1e). We see global annual maximum LSTs in the deserts and xeric shrublands biome, mainly in the Sonoran Desert, Gariep Karoo Desert, Djibouti xeric shrublands, North Arabian Desert, Central Persian Desert basins, and South Iran Nubo-Sindian Desert (or the Lut Desert mentioned earlier) (Dinerstein et al. 2017) (Figs. 1a,d and ES2a). These deserts are found under the subtropical ridge, where stable descending air and high pressure aloft favor hot, rainless, and arid conditions.

The Lut Desert stands out among all deserts with the world's highest LST and the highest number of yearly maximum LSTs, confirming the fact that it is one of the hottest places on Earth (Figs. 1a,b). This exceptional feature of the Lut Desert can be explained by its mountain-surrounded terrain, which limits air movement and enhances heat trapping, and its heat-absorbing blackened sand from volcanic lava. LST estimates in the Lut Desert are about 10°C higher compared with LSTs reported by Mildrexler et al. (2011b) in the same region. One reason could be due to the higher spatial resolution and better accuracy of the V6 MODIS LST product, used in this study, relative to the previous versions. Further, our study period covers a much longer period of time, relative to that of Mildrexler et al. (2011b), who examined 6 years

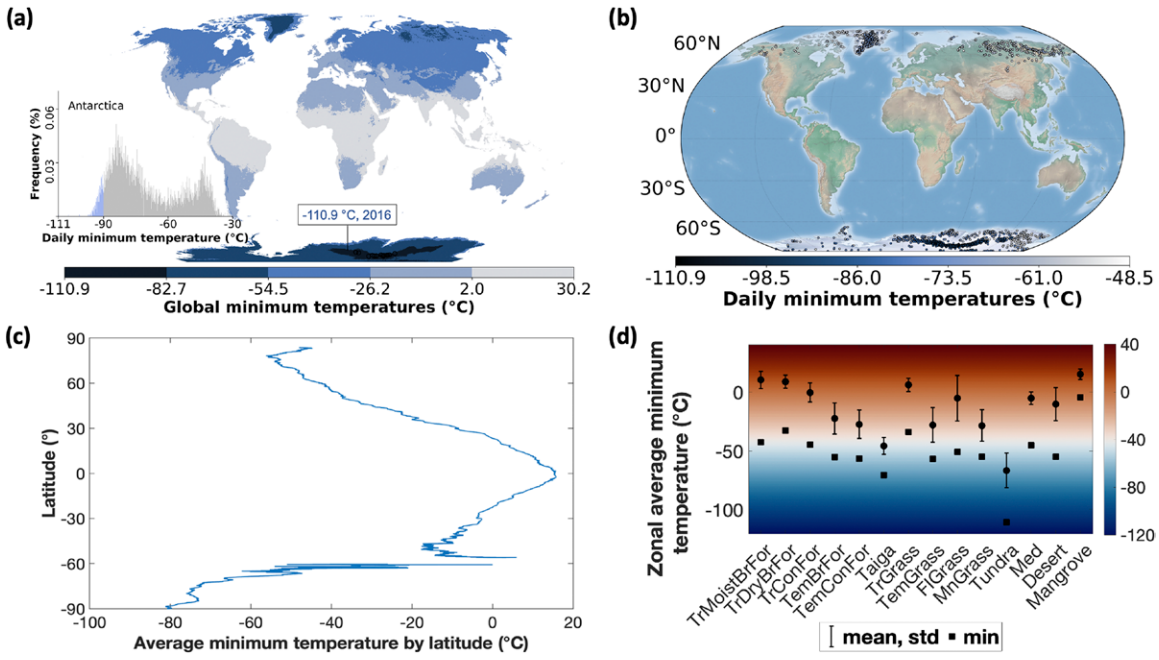

Fig. 2. Magnitudes and spatial distributions of the annual and daily minimum LSTs. (a)–(d) As in Figs. 1a, 1b, 1d, and 1e, but for minimum LSTs. The histogram in (a) shows the frequency distribution of daily minimum LSTs in Antarctica during the study period. The blue area indicates temperatures below –90°C. The percentage of days with daily minimum LSTs below –90°C in Antarctica is 5.7%.

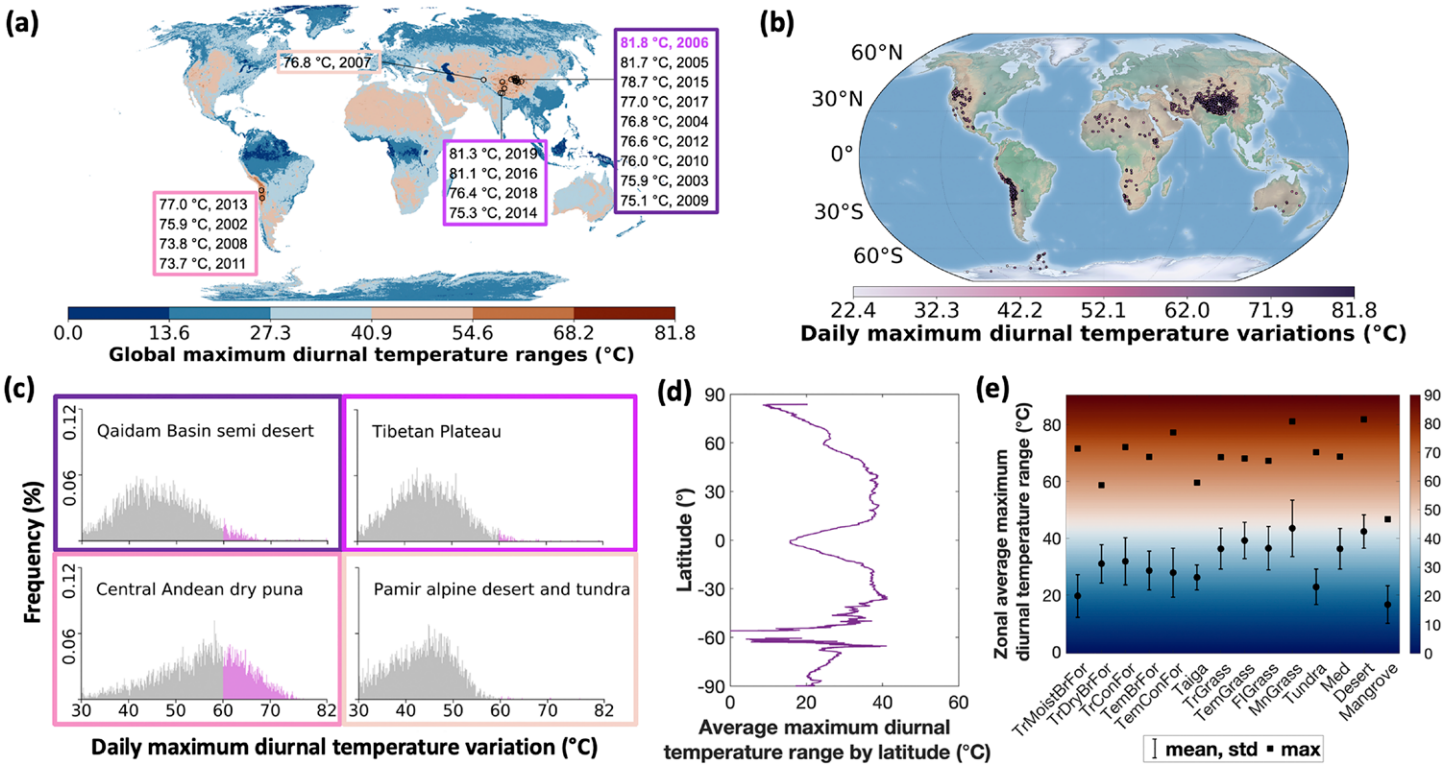

Fig. 3. Magnitudes and spatial distributions of the annual and daily maximum DTRs. (a)–(e) As in Figs. 1a–e, but for maximum DTRs. The histograms in (c) show the frequency distributions of daily maximum DTRs of the four diurnally most variable places on Earth during the study period. The purple areas indicate DTRs above 60°C. The percentages of days with daily maximum DTRs above 60°C are 4.9%, 1.7%, 33.1%, and 0.3% in the Qaidam Basin semidesert, the Tibetan Plateau, the central Andean dry puna, the Pamir alpine desert, and tundra, respectively.

of LSTs (2003–09). In fact, the highest observed record temperatures reported here have occurred in more recent years (2018 and 2019—see Fig. 1a). Finally, the observed atmospheric warming over the years (IPCC 2018) may have also contributed to higher LSTs in recent years, although this impact cannot be simply separated from natural variability.

The Sonoran Desert where the world's highest LST and the second-largest number of yearly maximum LSTs occur is mainly a rain shadow desert. Its relatively low elevation limits the effects of high-altitude cooling. Also, surrounded by mountains, heat is often trapped within the desert basin increasing both land and atmospheric temperatures. It is noteworthy that the observed annual maximum LSTs that occurred in the Sonoran Desert (July 2009, June 2016, July 2011, and August 2003) coincide with La Niña episodes based on the Southern Oscillation index (SOI). While both the Lut Desert and the Sonoran Desert have very similar annual maxima, considering the entire distribution of temperatures, Lut Desert is significantly warmer and extreme temperatures occur more frequently there than any other place on Earth (see the shaded area in Fig. 1c, which shows the temperature distributions of the four hottest places on Earth).

Results show a pronounced dip in latitudinal average maximum LSTs near the equator (Figs. 1a,d). Overall, daily maximum LST peaks near the tropics of Cancer and Capricorn, and it diminishes further toward the equator. The latitudinal pattern in maximum LSTs reflects the regional climate (e.g., shortwave radiation, longwave emittance, rainfall) and biophysical regulation (e.g., albedo, evapotranspiration) in determining the general spatial patterns of hot extremes (Bonan 2008; Gibbard et al. 2005; Li et al. 2015). The consistent high temperature in subtropical deserts is mainly because of the nearly constant high pressure aloft over subtropics, which enhances subsidence, solar heating, and advection in heat transfer, and prevents low pressure airflow from rising. The latter significantly reduces the chance of precipitation. The land surfaces in the deserts and xeric shrublands are water limited and

cannot cool down because of intense solar radiation and shortage of water for evaporation, contributing to their observed extremely hot LSTs. We observe the highest magnitude and the lowest standard deviation of zonal average maximum LSTs in the deserts and xeric shrublands biome (Fig. 1e). The tundra biome, subject to weak solar radiation (energy limited) but rich in water for evapotranspiration, featured with patchy distributions of grasses and shrubs (Mildrexler et al. 2018; Nemani and Running 1997; Mildrexler et al. 2011a), is characterized by the lowest magnitude and highest standard deviation of zonal average maximum LSTs of −2.4° ± 18.4°C. In the forest biome, the relatively lower LSTs are primarily because of cooling processes associated with evapotranspiration, which dissipates absorbed shortwave solar energy as latent heat flux (Mildrexler et al. 2018; Nemani and Running 1997).

Global pattern of daily minimum temperature. As expected, the global daily minimum LSTs during the study period occurs in Antarctica, the Arctic and tundra regions (Fig. 2b) and the annual minimum LSTs only occur in Antarctica (Figs. 2a and ES2b) where the incoming solar radiation is weak and a large portion of it is reflected back from the surface snow cover and ice sheets. Further, Antarctica is surrounded by oceans, typically controlled by low-pressure systems. This leads to strong winds from the center of the continent to its margins, contributing to record cold extremes. With the lowest observed LST of −110.9°C, central-eastern Antarctica is the world's coldest region. The record low LST in Antarctica is around 20°C lower than the world's record low atmospheric temperature of −89.2°C reported by WMO.

Latitudinal average minimum LSTs are the highest at the equator and decrease roughly monotonically northward and southward (Figs. 2a,c). This latitudinal pattern in minimum LSTs reflects the amount of energy stored during the daytime (Peng et al. 2014), which is jointly determined by the climate (e.g., shortwave radiation, rainfall) and biophysical regulation (e.g., albedo, heat capacity) (Li et al. 2015). Receiving weak solar radiation in the daytime, the high-latitude patchy tundra biome stores little energy and features the lowest magnitude and high standard deviation of zonal average minimum LSTs of −66.6° ± 14.8°C (Fig. 2d). This contrasts with the high magnitude and low standard deviation of zonal average minimum LST of 10.5° ± 7.2°C in the high-density tropical and subtropical moist broadleaf forests (Fig. 2d) where a considerable amount of energy can be stored. On the other hand, deserts and xeric shrublands generally have a high albedo and reflect a large amount of incoming radiation. Further, their low heat capacity (as a result of lack of water) release heat rapidly at night. As a result, their zonal average minimum LST is as low as −10.1° ± 14.1°C (Fig. 2d).

Global pattern of diurnal temperature range. After investigating the hottest and coldest places on Earth, we turn our attention to extreme DTRs around the world. We observe the global daily maximum DTRs mainly in two biomes: the deserts and xeric shrublands and the tropical and subtropical grasslands, savannas and shrublands (Fig. 3b). In contrast to daily maximum LSTs, which typically occur in hot deserts (Fig. 1b), the daily maximum DTRs occur in cold deserts. During the study period, the annual maximum DTRs have occurred in the Qaidam Basin (China), central Tibetan Plateau alpine steppe, Western Himalayan alpine shrub and meadows, Central Asian southern desert, and central Andean dry puna (Dinerstein et al. 2017) (Figs. 3a and ES2c). The most extreme DTR of 81.8°C is observed in the Qaidam Basin in China. Like maximum and minimum LSTs, the magnitude of DTR also reflects the joint regulation of biomes by climate (e.g., shortwave radiation, rainfall, vapor pressure) and biophysical properties (e.g., albedo, heat capacity) (Peng et al. 2014; Li et al. 2015). With low heat capacity (as a result of lack of soil moisture), the barren soil in the Qaidam Basin absorbs heat fast in the daytime. As a region with limited water resources, extremely high LSTs are caused by the trapped heat that cannot be dissipated through evaporation. At night, the low heat capacity and air humidity in the Qaidam Basin prompt the leakage of

longwave radiation, which leads to rapid cooling in the Qaidam Basin. In addition, as it is surrounded by high-elevation mountains such as the Kunlun Mountains (23,514 ft), the cold air (low vapor pressure at high altitude leads to low air moisture, thus a considerable amount of heat is released through outgoing longwave radiation) from high altitudes moves downward, further cooling the area, resulting in extremely cold LST. While the Qaidam Basin appears to have the record DTR, considering a particular extreme DTR threshold (e.g., 60°C), the central Andean dry puna exhibits more frequent extreme DTR variability (see the shaded area in Fig. 3c, which shows the DTR distributions of the diurnally most variable places on Earth).

The latitudinal pattern of the global maximum DTR is more complex than hot and cold LSTs. The latitudinally average maximum DTR is lowest in the polar regions, and increases toward the low latitudes, peaking near the tropics of Cancer and Capricorn, and then declines toward the equator (Fig. 3d). Both forest and xeric and desert biomes are found in low latitudes, subject to intense solar radiation. However, because of biophysical difference (mainly heat capacity and air moisture), the maximum DTRs in forests are significantly lower than those in deserts (Fig. 3e).

Conclusions

In this paper, we show that the Lut Desert in Iran and the Sonoran Desert in Mexico are the hottest places on Earth with a land surface temperature (LST) of 80.8°C—a record temperature that is over 10°C hotter than the previous global skin temperature record. The world's lowest LST of −110.9°C is observed in Antarctica, whereas the maximum global diurnal temperature range (DTR) of 81.8°C is observed in the Qaidam Basin in China. Biomes around the world show a very high level of variability with respect to extremes. We detect the highest zonal average maximum LST of 61.1° ± 5.3°C in the deserts and xeric shrublands. The lowest zonal average minimum LST of −66.6° ± 14.8°C is found in the tundra, whereas the highest zonal average maximum DTR of 43.5° ± 9.9°C is identified in the montane grasslands and shrublands.

Earth has been warming and temperatures are projected to increase even more in the future. Human-caused warming may have already contributed to the highest global LST observed in the Lut Desert and the Sonoran Desert. However, the anthropogenic contribution cannot be simply separated from natural variability. Considering the land–atmosphere interactions (Miralles et al. 2014; Fischer and Schär 2008; Seneviratne et al. 2006), rising atmospheric temperatures will likely lead to even higher temperature extremes. Temperature extremes, including high diurnal variability, could also influence diverse ecological and environmental processes from biological changes (Yeaman et al. 2016; Sunday et al. 2014) to thermal stress on plants and animals (Hughes et al. 2018; Iknayan and Beissinger 2018), interspecific relationships (García et al. 2018), and disease (e.g., malaria) transmission (Paaijmans et al. 2010). A global assessment of the extent to which biomes are faced with temperature extremes is increasingly more important as the atmospheric warming continues. While the behavior of the atmosphere in response to more anthropogenic emissions is well studied (Lacis et al. 2010; Tyndall 1863; Karl 2003), the response of the land surface under different emission pathways is not well understood. It is hoped the future research in this direction can shed light on not only how extremes have changed in the past but how they will likely affect our planet in the future.

Acknowledgments. This study was supported by NASA Award NNX15AC27G and NSF Award OAC-1931335.

Data availability statement. All data used in this study are publicly available: land surface temperature data (https://lpdaac.usgs.gov/products/myd11a1v006/), fire data (https://lpdaac.usgs.gov/products/myd14a1v006/), and biome data (https://ecoregions2017.appspot.com/). These data were accessed through the Google Earth Engine cloud computing platform (Gorelick et al. 2017). All data analysis codes will be made available to researchers interested to reproduce the results. The authors declare no competing interests.

References

Azarderakhsh, M., S. Prakash, Y. Zhao, and A. AghaKouchak, 2020: Satellite-based analysis of extreme land surface temperatures and diurnal variability across the hottest place on Earth. *IEEE Geosci. Remote Sens. Lett.*, **17**, 2025–2029, https://doi.org/10.1109/LGRS.2019.2962055.

Arizona State University, 2020: World Meteorological Organization's World Weather & Climate Extremes Archive. Accessed 8 January 2020, https://wmo.asu.edu/content/mapviewer.

Benz, S. A., S. J. Davis, and J. Burney, 2021: Drivers and projections of global surface temperature anomalies at sub-city scale. OSF Preprints, https://doi.org/10.31219/osf.io/a8rfx.

Bonan, G. B., 2008: Forests and climate change: Forcings, feedbacks, and the climate benefits of forests. *Science*, **320**, 1444–1449, https://doi.org/10.1126/science.1155121.

Cohen, J., and Coauthors, 2014: Recent Arctic amplification and extreme mid-latitude weather. *Nat. Geosci.*, **7**, 627–637, https://doi.org/10.1038/ngeo2234.

Coll, C., V. Caselles, J. M. Galve, E. Valor, R. Niclòs, J. M. Sánchez, and R. Rivas, 2005: Ground measurements for the validation of land surface temperatures derived from AATSR and MODIS data. *Remote Sens. Environ.*, **97**, 288–300, https://doi.org/10.1016/j.rse.2005.05.007.

——, Z. Wan, and J. M. Galve, 2009: Temperature-based and radiance-based validations of the V5 MODIS land surface temperature product. *J. Geophys. Res.*, **114**, D20102, https://doi.org/10.1029/2009JD012038.

Crameri, F., 2018: Scientific colour maps: Perceptually uniform and colour-vision deficiency friendly. Zenodo, https://doi.org/10.5281/zenodo.1243862.

——, G. E. Shephard, and P. J. Heron, 2020: The misuse of colour in science communication. *Nat. Commun.*, **11**, 5444, https://doi.org/10.1038/s41467-020-19160-7.

Dinerstein, E., and Coauthors, 2017: An ecoregion-based approach to protecting half the terrestrial realm. *BioScience*, **67**, 534–545, https://doi.org/10.1093/biosci/bix014.

Duan, S. B., Z. L. Li, H. Wu, P. Leng, M. Gao, and C. Wang, 2018: Radiance-based validation of land surface temperature products derived from collection 6 MODIS thermal infrared data. *Int. J. Appl. Earth Obs. Geoinf.*, **70**, 84–92, https://doi.org/10.1016/j.jag.2018.04.006.

——, and Coauthors, 2019: Validation of collection 6 MODIS land surface temperature product using in situ measurements. *Remote Sens. Environ.*, **225**, 16–29, https://doi.org/10.1016/j.rse.2019.02.020.

Fischer, E. M., and C. Schär, 2008: Future changes in daily summer temperature variability: Driving processes and role for temperature extremes. *Climate Dyn.*, **33**, 917–935, https://doi.org/10.1007/s00382-008-0473-8.

García, F. C., E. Bestion, R. Warfield, and G. Yvon-Durocher, 2018: Changes in temperature alter the relationship between biodiversity and ecosystem functioning. *Proc. Natl. Acad. Sci. USA*, **115**, 10 989–10 994, https://doi.org/10.1073/pnas.1805518115.

Gibbard, S., K. Caldeira, G. Bala, T. J. Phillips, and M. Wickett, 2005: Climate effects of global land cover change. *Geophys. Res. Lett.*, **32**, L23705, https://doi.org/10.1029/2005GL024550.

Giglio, L., W. Schroeder, and C. O. Justice, 2016: The collection 6 MODIS active fire detection algorithm and fire products. *Remote Sens. Environ.*, **178**, 31–41, https://doi.org/10.1016/j.rse.2016.02.054.

Good, E. J., 2016: An in situ-based analysis of the relationship between land surface "skin" and screen-level air temperatures. *J. Geophys. Res. Atmos.*, **121**, 8801–8819, https://doi.org/10.1002/2016JD025318.

Gorelick, N., M. Hancher, M. Dixon, S. Ilyushchenko, D. Thau, and R. Moore, 2017: Google Earth Engine: Planetary-scale geospatial analysis for everyone. *Remote Sens. Environ.*, **202**, 18–27, https://doi.org/10.1016/j.rse.2017.06.031.

Hughes, T. P., and Coauthors, 2018: Global warming transforms coral reef assemblages. *Nature*, **556**, 492–496, https://doi.org/10.1038/s41586-018-0041-2.

Iknayan, K. J., and S. R. Beissinger, 2018: Collapse of a desert bird community over the past century driven by climate change. *Proc. Natl. Acad. Sci. USA*, **115**, 8597–8602, https://doi.org/10.1073/pnas.1805123115.

IPCC, 2018: Global Warming of 1.5°C: An IPCC Special Report on the impacts of global warming of 1.5°C above pre-industrial levels and related global greenhouse gas emission pathways, in the context of strengthening the global response to the threat of climate change, sustainable development, and efforts to eradicate poverty. V. Masson-Delmotte et al., Eds., IPCC, 616 pp., www.ipcc.ch/sr15/.

Johnson, N. C., S.-P. Xie, Y. Kosaka, and X. Li, 2018: Increasing occurrence of cold and warm extremes during the recent global warming slowdown. *Nat. Commun.*, **9**, 1724, https://doi.org/10.1038/s41467-018-04040-y.

Karl, T. R., 2003: Modern global climate change. *Science*, **302**, 1719–1723, https://doi.org/10.1126/science.1090228.

Kodra, E., K. Steinhaeuser, and A. R. Ganguly, 2011: Persisting cold extremes under 21st-century warming scenarios. *Geophys. Res. Lett.*, **38**, L08705, https://doi.org/10.1029/2011GL047103.

Kretschmer, M., D. Coumou, L. Agel, M. Barlow, E. Tziperman, and J. Cohen, 2018: More-persistent weak stratospheric polar vortex states linked to cold extremes. *Bull. Amer. Meteor. Soc.*, **99**, 49–60, https://doi.org/10.1175/BAMS-D-16-0259.1.

Lacis, A. A., G. A. Schmidt, D. Rind, and R. A. Ruedy, 2010: Atmospheric CO_2: Principal control knob governing Earth's temperature. *Science*, **330**, 356–359, https://doi.org/10.1126/science.1190653.

Li, Y., M. Zhao, S. Motesharrei, Q. Mu, E. Kalnay, and S. Li, 2015: Local cooling and warming effects of forests based on satellite observations. *Nat. Commun.*, **6**, 6603, https://doi.org/10.1038/ncomms7603.

Li, Z.-L., B.-H. Tang, H. Wu, H. Ren, G. Yan, Z. Wan, I. F. Trigo, and J. A. Sobrino, 2013: Satellite-derived land surface temperature: Current status and perspectives. *Remote Sens. Environ.*, **131**, 14–37, https://doi.org/10.1016/j.rse.2012.12.008.

Liu, Z., A. P. Ballantyne, and L. A. Cooper, 2019: Biophysical feedback of global forest fires on surface temperature. *Nat. Commun.*, **10**, 214, https://doi.org/10.1038/s41467-018-08237-z.

Luo, D., X. Chen, J. Overland, I. Simmonds, Y. Wu, and P. Zhang, 2019: Weakened potential vorticity barrier linked to recent winter arctic sea ice loss and mid-latitude cold extremes. *J. Climate*, **32**, 4235–4261, https://doi.org/10.1175/JCLI-D-18-0449.1.

Mildrexler, D. J., M. Zhao, and S. W. Running, 2011a: A global comparison between station air temperatures and MODIS land surface temperatures reveals the cooling role of forests. *J. Geophys. Res. Biogeosci.*, **116**, G03025, https://doi.org/10.1029/2010JG001486.

——,——, and ——, 2011b: Satellite finds highest land skin temperatures on Earth. *Bull. Amer. Meteor. Soc.*, **92**, 855–860, https://doi.org/10.1175/2011BAMS3067.1.

——, ——, W. B. Cohen, S. W. Running, X. P. Song, and M. O. Jones, 2018: Thermal anomalies detect critical global land surface changes. *J. Appl. Meteor. Climatol.*, **57**, 391–411, https://doi.org/10.1175/JAMC-D-17-0093.1.

Miralles, D. G., A. J. Teuling, C. C. van Heerwaarden, and J. Vilà-Guerau de Arellano, 2014: Mega-heatwave temperatures due to combined soil desiccation and atmospheric heat accumulation. *Nat. Geosci.*, **7**, 345–349, https://doi.org/10.1038/ngeo2141.

Munich RE, 2019: NatCatSERVICE analysis tool. Accessed 17 October 2019, www.munichre.com/en/risks.html.

Nemani, R., and S. Running, 1997: Land cover characterization using multitemporal red, near-IR, and thermal-IR data from NOAA/AVHRR. *Ecol. Appl.*, **7**, 79–90, https://doi.org/10.1890/1051-0761(1997)007[0079:LCCUMR]2.0.CO;2.

Nie, S., S. Fu, W. Cao, and X. Jia, 2020: Comparison of monthly air and land surface temperature extremes simulated using CMIP5 and CMIP6 versions of the Beijing Climate Center climate model. *Theor. Appl. Climatol.*, **140**, 487–502, https://doi.org/10.1007/s00704-020-03090-x.

Oudin Åström, D., B. Forsberg, K. L. Ebi, and J. Rocklöv, 2013: Attributing mortality from extreme temperatures to climate change in Stockholm, Sweden. *Nat. Climate Change*, **3**, 1050–1054, https://doi.org/10.1038/nclimate2022.

Paaijmans, K. P., S. Blanford, A. S. Bell, J. I. Blanford, A. F. Read, and M. B. Thomas, 2010: Influence of climate on malaria transmission depends on daily temperature variation. *Proc. Natl. Acad. Sci. USA*, **107**, 15 135–15 139, https://doi.org/10.1073/pnas.1006422107.

Papritz, L., 2020: Arctic lower-tropospheric warm and cold extremes: Horizontal and vertical transport, diabatic processes, and linkage to synoptic circulation features. *J. Climate*, **33**, 993–1016, https://doi.org/10.1175/JCLI-D-19-0638.1.

Peng, S., and Coauthors, 2013: Asymmetric effects of daytime and night-time warming on Northern Hemisphere vegetation. *Nature*, **501**, 88–92, https://doi.org/10.1038/nature12434.

Peng, S. S., and Coauthors, 2014: Afforestation in China cools local land surface temperature. *Proc. Natl. Acad. Sci. USA*, **111**, 2915–2919, https://doi.org/10.1073/pnas.1315126111.

Schwartz, J., 2005: Who is sensitive to extremes of temperature? A case-only analysis. *Epidemiology*, **16**, 67–72, https://doi.org/10.1097/01.ede.0000147114.25957.71.

Seneviratne, S. I., D. Lüthi, M. Litschi, and C. Schär, 2006: Land–atmosphere coupling and climate change in Europe. *Nature*, **443**, 205–209, https://doi.org/10.1038/nature05095.

Sharifnezhadazizi, Z., H. Norouzi, S. Prakash, C. Beale, and R. Khanbilvardi, 2019: A global analysis of land surface temperature diurnal cycle using MODIS observations. *J. Appl. Meteor. Climatol.*, **58**, 1279–1291, https://doi.org/10.1175/JAMC-D-18-0256.1.

Sunday, J. M., A. E. Bates, M. R. Kearney, R. K. Colwell, N. K. Dulvy, J. T. Longino, and R. B. Huey, 2014: Thermal-safety margins and the necessity of thermoregulatory behavior across latitude and elevation. *Proc. Natl. Acad. Sci. USA*, **111**, 5610–5615, https://doi.org/10.1073/pnas.1316145111.

Tang, Q., X. Zhang, X. Yang, and J. A. Francis, 2013: Cold winter extremes in northern continents linked to Arctic sea ice loss. *Environ. Res. Lett.*, **8**, 014036, https://doi.org/10.1088/1748-9326/8/1/014036.

Tyndall, J., 1863: XXVII. On radiation through the earth's atmosphere. *London Edinburgh Dublin Philos. Mag. J. Sci.*, **25**, 200–206, https://doi.org/10.1080/14786446308643443.

Wan, Z., 2008: New refinements and validation of the MODIS land-surface temperature/emissivity products. *Remote Sens. Environ.*, **112**, 59–74, https://doi.org/10.1016/j.rse.2006.06.026.

——, 2013: Collection-6 MODIS land surface temperature products users' guide. University of California, Santa Barbara, 33 pp., https://lpdaac.usgs.gov/documents/118/MOD11_User_Guide_V6.pdf.

——, 2014: New refinements and validation of the collection-6 MODIS land-surface temperature/emissivity product. *Remote Sens. Environ.*, **140**, 36–45, https://doi.org/10.1016/j.rse.2013.08.027.

——, and Z.-L. Li, 2008: Radiance-based validation of the V5 MODIS land-surface temperature product. *Int. J. Remote Sens.*, **29**, 5373–5395, https://doi.org/10.1080/01431160802036565.

——, Y. Zhang, Q. Zhang, and Z.-L. Li, 2004: Quality assessment and validation of the MODIS global land surface temperature. *Int. J. Remote Sens.*, **25**, 261–274, https://doi.org/10.1080/0143116031000116417.

——, S. Hook, and G. Hulley, 2015: MYD11A1 MODIS/*Aqua* Land Surface Temperature/Emissivity Daily L3 Global 1 km SIN Grid V006. NASA EOSDIS Land Processes DAAC, accessed 8 January 2020, https://doi.org/10.5067/MODIS/MYD11A1.006.

Wang, K., and S. Liang, 2009: Evaluation of ASTER and MODIS land surface temperature and emissivity products using long-term surface longwave radiation observations at SURFRAD sites. *Remote Sens. Environ.*, **113**, 1556–1565, https://doi.org/10.1016/j.rse.2009.03.009.

——, Z. Wan, P. Wang, M. Sparrow, J. Liu, and S. Haginoya, 2007: Evaluation and improvement of the MODIS land surface temperature/emissivity products using ground-based measurements at a semi-desert site on the western Tibetan Plateau. *Int. J. Remote Sens.*, **28**, 2549–2565, https://doi.org/10.1080/01431160600702665.

Xie, W., and Coauthors, 2018: Decreases in global beer supply due to extreme drought and heat. *Nat. Plants*, **4**, 964–973, https://doi.org/10.1038/s41477-018-0263-1.

Yeaman, S., and Coauthors, 2016: Convergent local adaptation to climate in distantly related conifers. *Science*, **353**, 1431–1433, https://doi.org/10.1126/science.aaf7812.

Zhou, C., and K. Wang, 2016: Land surface temperature over global deserts: Means, variability, and trends. *J. Geophys. Res. Atmos.*, **121**, 14 344–14 357, https://doi.org/10.1002/2016JD025410.

Zhou, L., H. Chen, and Y. Dai, 2015: Stronger warming amplification over drier ecoregions observed since 1979. *Environ. Res. Lett.*, **10**, 064012, https://doi.org/10.1088/1748-9326/10/6/064012.